Letter

Dynamical signatures of thermal spin-charge deconfinement in the doped Ising model

Lauritz Hahn [1,2] Annabelle Bohrdt,[3,4] and Fabian Grusdt [1,2,*]

[1]*Department of Physics and Arnold Sommerfeld Center for Theoretical Physics (ASC), Ludwig-Maximilians-Universität München, Theresienstraße 37, München D-80333, Germany*

[2]*Munich Center for Quantum Science and Technology (MCQST), Schellingstraße 4, D-80799 München, Germany*

[3]*ITAMP, Harvard-Smithsonian Center for Astrophysics, Cambridge, Massachusetts 02138, USA*

[4]*Department of Physics, Harvard University, Cambridge, Massachusetts 02138, USA*

(Received 26 September 2021; revised 25 April 2022; accepted 8 June 2022; published 27 June 2022)

The mechanism underlying charge transport in strongly correlated quantum systems, such as doped antiferromagnetic Mott insulators, remains poorly understood. Here, we study the expansion dynamics of an initially localized hole inside a two-dimensional (2D) Ising antiferromagnet at variable temperature. Using a combination of classical Monte Carlo and truncated-basis methods, we reveal two dynamically distinct regimes: a spin-charge confined region below a critical temperature T^*, characterized by slow spreading, and a spin-charge deconfined region above T^*, characterized by an unbounded diffusive expansion. The deconfinement temperature $T^* \approx 0.65 J_z$ we find is around the Néel temperature $T_N = 0.567 J_z$ of the Ising background in 2D, but we expect $T^* < T_N$ in higher dimensions. In both regimes we find that the mobile hole does not thermalize with the Ising spin background on the considered time scales, indicating weak effective coupling of spin and charge degrees of freedom. Our results can be qualitatively understood by an effective parton model and can be tested experimentally in state-of-the-art quantum gas microscopes.

DOI: 10.1103/PhysRevB.105.L241113

Introduction. In the field of high-T_c superconductivity emerging from correlated insulating parent states [1], understanding the properties of individual charge carriers in doped two-dimensional (2D) antiferromagnets has been a central goal. While a magnetic, or spin, polaron forms at low doping, experiments observe a crossover from a polaronic metal at low doping to a Fermi liquid at high doping [2]. Although the ground-state properties of magnetic polarons at low doping are essentially agreed upon [3–11], their fate at elevated temperatures or nonzero doping, as well as their far-from-equilibrium dynamics, remains poorly understood.

Recently, ultracold-atom experiments have ventured into this regime [12]. In equilibrium, the dressing cloud of a magnetic polaron has been observed for the first time [13], and the dynamical spreading of an initially localized hole in 2D has revealed a significant slowdown associated with the presence of spin correlations [14]. Theoretical work on the dynamical properties of doped holes has revealed signatures of parton [15] and string formation [15–19] at low temperatures and predicted diffusive or subdiffusive spreading at infinite temperatures depending on the interactions between the spins [15,20,21].

Here, we study the nonequilibrium dynamics of an initially localized single dopant in a thermal 2D Ising background; see Fig. 1(a). While previous studies addressed this problem in the limits of infinite temperature with [15] or without [20,21] Ising interactions J_z, and at zero temperature with Ising couplings [22], we systematically tune the temperature T across the Ising critical point at $T_N = 0.567 J_z$. Combining numerical Monte Carlo and truncated-basis methods, we reveal two regimes with qualitatively distinct hole dynamics; see Fig. 1. By comparing our results with an effective parton model, we argue that the low-temperature behavior corresponds to spin-charge confinement, whereas spin and charge are deconfined at high temperatures; see Fig. 1(d).

Furthermore, we study the thermalization dynamics of the mobile hole. We find that after a few tunneling times the hole quickly realizes a steady state which differs significantly from the thermal state, especially in the deconfined regime at high temperatures. This finding is interesting since the t-J_z model is neither believed to be integrable nor localizing [23,24].

Model. Some of the most relevant aspects of hole dynamics in antiferromagnetic (AFM) environments can be captured by the t-J_z Hamiltonian [22,25] in $d = 2$ dimensions,

$$\hat{\mathcal{H}} = -t \sum_{\langle i,j\rangle,\sigma} \hat{\mathcal{P}}(\hat{c}^\dagger_{i,\sigma}\hat{c}_{j,\sigma} + \text{H.c.})\hat{\mathcal{P}} + J_z \sum_{\langle i,j\rangle} \hat{S}^z_i \hat{S}^z_j, \quad (1)$$

where the first term $\hat{\mathcal{H}}_t$ is the nearest-neighbor (NN) hopping with amplitude t, $\hat{c}_{j,\sigma}$ annihilates a fermion of spin σ at site j, and $\hat{\mathcal{P}}$ is a projector to the subspace without double occupancies. The second term $\hat{\mathcal{H}}_{J_z}$ denotes NN AFM Ising interactions of the spins $\hat{S}^z_j = \sum_\sigma (-1)^\sigma \hat{c}^\dagger_{j,\sigma}\hat{c}_{j,\sigma}$ with strength $J_z > 0$.

While the t-J_z model constitutes a strong simplification, it captures several aspects relevant to experiments on strongly correlated electrons in cuprates, e.g., the formation of string patterns [22,23,26]. Although the Ising background $\hat{\mathcal{H}}_{J_z}$ itself is classical, the noncommuting hopping term $\hat{\mathcal{H}}_t$ allows

*Corresponding author: fabian.grusdt@physik.uni-muenchen.de

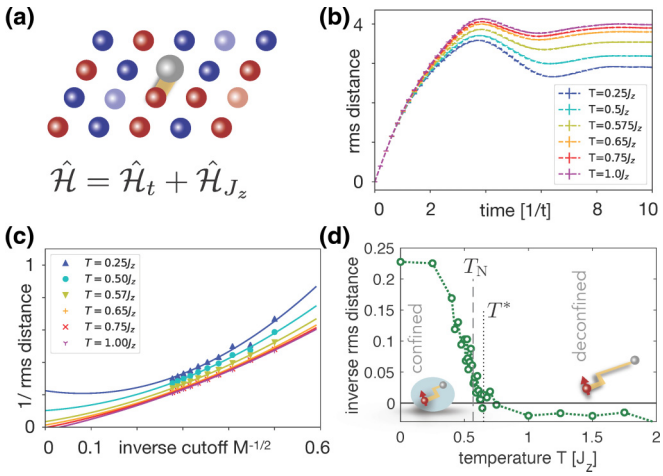

FIG. 1. We study the spreading of an initially localized hole in a thermal Ising background at temperatures T (a). The root-mean-square (rms) distance from the origin, shown for $M = 10$, reveals slow (fast) spreading at low (high) temperatures (b). We study the long-time value of the inverse rms distance to extrapolate its value in the thermodynamic limit when our finite-size cutoff $M \to \infty$ (c); for high T the data almost collapse. Plotting the result for different temperatures (d) reveals a dynamically confined (deconfined) regime at low (high) temperatures. We show plots for $t/J_z = 3$.

one to couple most spin states to each other already by a single mobile dopant; even in a perfect Néel background at zero temperature, Trugman loops lead to coherent hole motion [22,24,27]. This renders $\hat{\mathcal{H}}$ a truly quantum Hamiltonian.

In the following, we study quantum quenches starting from an undoped thermal Ising state described by the density matrix $\hat{\rho}_0 = e^{-\beta\hat{\mathcal{H}}_{J_z}}/Z_0$, where $\beta = 1/T$ is the inverse of temperature T and we set $k_B = 1$. At time $\tau = 0$ a single hole is created in the origin at $\boldsymbol{j} = \mathbf{0}$, and the initial state is $\hat{\rho}(0) = \sum_\sigma \hat{c}_{\mathbf{0},\sigma}\,\hat{\rho}_0\,\hat{c}^\dagger_{\mathbf{0},\sigma}$.

Numerical technique. To calculate the time-evolved density matrix $\hat{\rho}(\tau)$ with a single hole, we leverage the classical nature of the Ising background $\hat{\mathcal{H}}_{J_z}$. Specifically, we sample thermal initial spin states, dope them with one hole, and calculate their time evolution by a truncated-basis method [16,17,28].

For a given eigenstate $|\Psi^n\rangle$ of the 2D Ising Hamiltonian, we obtain an initial one-hole state $|\psi^n_1\rangle = \hat{c}_{\mathbf{0},\sigma_\mathbf{0}}|\Psi^n\rangle$ by removing the fermion at the origin with spin $\sigma_\mathbf{0}$. Repeated applications of the terms in $\hat{\mathcal{H}}_t$ then generate new states which we add to the truncated basis $\{|\psi^n_\nu\rangle\}_{\nu=1\cdots d_M}$ used for numerical time evolution. In this process, orthonormality is guaranteed by projecting each new state onto all previous states. Since $\hat{\mathcal{H}}_t$ is applied in each step, the total number of iterations M corresponds to the largest number of hops the hole can perform in the truncated basis without retracing its path; the dimension d_M of the truncated basis grows exponentially with M and depends on the initial configuration n.

To study the thermal properties of the expansion dynamics, the thermal average over the ensemble of background spin states $\{|\Psi^n\rangle\}_{n=1\cdots N}$—i.e., the ensemble of the Ising model at a given temperature T—must be performed. We achieve this using a standard Metropolis Monte Carlo algorithm to obtain a large number ($N = 100$) of representative samples for desired temperatures T. For each of these samples $|\Psi^n\rangle$, the corresponding truncated base $\{|\psi^n_\nu\rangle\}_\nu$ is generated, and the Schrödinger equation is solved on the restricted subspace starting from the initial state $|\psi^n(\tau = 0)\rangle = |\psi^n_1\rangle \equiv \hat{c}_{\mathbf{0},\sigma_\mathbf{0}}|\Psi^n\rangle$.

Estimators for expectation values of observables such as the root-mean-square (rms) distance of the hole from the origin $r_{\rm rms}$ can then be obtained by averaging the results obtained for each sample n,

$$r_{\rm rms}(\tau) \approx \frac{1}{N}\sum_{n=1}^{N}\left(\sum_{\boldsymbol{j}} \boldsymbol{j}^2 \langle\psi^n(\tau)|\hat{n}^h_{\boldsymbol{j}}|\psi^n(\tau)\rangle\right)^{1/2}, \qquad (2)$$

with $\hat{n}^h_{\boldsymbol{j}} = \prod_\sigma(1 - \hat{c}^\dagger_{\boldsymbol{j},\sigma}\hat{c}_{\boldsymbol{j},\sigma})$ being the hole density on site $\boldsymbol{j}$ which we evaluate in the truncated basis.

Numerical results. In Fig. 1(b) we show typical numerically obtained time traces of the hole's rms distance, for $t/J_z = 3$ and $M = 10$. We observe slow spreading of the hole at low temperatures well below the Ising transition at $T_{\rm N}$ and faster spreading at high temperatures above $T_{\rm N}$. At longer times corresponding to a few tunneling events (typically, we go up to times $\tau_{\rm max} = 15/t$), both curves saturate. However, this is partly due to the finite dimension of the restricted basis we employ.

We analyze the dependence of the long-time limit $r^{-1}_{\rm rms}(\tau_{\rm max})$ on the number of iterations M, corresponding to the maximum number of allowed tunneling events, in Fig. 1(c). For high temperatures, we observe scaling consistent with $r^{-1}_{\rm rms}(\tau_{\rm max}) \simeq M^{-1/2}$, i.e., the rms distance grows quickly and indefinitely. A scaling $\simeq M^{-1/2}$ with the square root of the number of allowed steps is expected from a classical random walk; this is true even at zero temperature for $J_z = 0$ (see Ref. [21]).

On the other hand, for low temperatures compared with J_z, we find $r^{-1}_{\rm rms}(\tau_{\rm max}) \to {\rm const} > 0$ as $M^{-1/2} \to 0$, indicating slow spreading of the hole, bounded by a finite length scale $r^{\rm max}_{\rm rms}$ at time $\tau_{\rm max}$. We notice that for much longer times, on the order of $\tau_{\rm T} \gtrsim 100/t$ [22], Trugman loop effects are expected to lead to very slow but unbounded growth of $r_{\rm rms}$ [24]; however, these physics play no role on the time scales up to $\tau_{\rm max}$ considered here. Moreover, Trugman loops describe a correlated motion of spin and charge and hence cannot lead to spin-charge deconfinement on its own.

Finally, we repeat the procedure described above for more values of the temperature T, in particular, around the Néel transition temperature $T_{\rm N} = 0.567 J_z$. The resulting extrapolated $r^{-1}_{\rm rms}(T; \tau_{\rm max}, M^{-1/2} \to 0)$, by a quadratic fit, are plotted over temperature in Fig. 1(d). At a critical temperature around $T^* \approx 0.65 J_z$ close to but distinctly above $T_{\rm N}$, we find an abrupt change of behavior, with unbounded (bounded) growth of $r_{\rm rms}$ above (below) T^*. This is a main result of this Research Letter and, as discussed below, we interpret it as a dynamical signature of a confinement ($T < T^*$) to deconfinement ($T > T^*$) transition of the spin and charge sectors.

We performed a similar analysis as in Fig. 1 for a different value of $t/J_z = 1$. The extrapolated long-time inverse rms distances are compared with the previous case in Fig. 2. We find similar qualitative behavior, and remarkably, the transition temperature T^* does not change for different t/J_z. Overall the

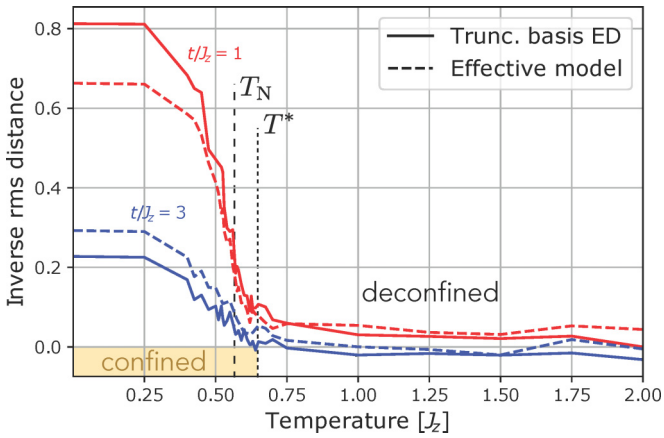

FIG. 2. We show long-time rms distances of a single hole extrapolated to $M^{-1/2} \to 0$ as a function of temperature, $r_{\rm rms}(T; \tau_{\rm max}, M^{-1/2} \to 0)$, for two ratios of $t/J_z = 1$ (upper solid curve) and $t/J_z = 3$ (lower solid curve). We compare our results with predictions by an effective spinon-chargon model (dashed curves) capturing the qualitative behavior. We indicate $T_{\rm N}$ and our estimate for $T^* = 0.65 J_z$ by vertical lines. ED, exact diagonalization; Trunc., truncated.

charge dynamics is only weakly affected by the spin background for $T > T^*$, while it depends strongly on the value of J_z/t when $T < T^*$. These observations indicate a strikingly different interplay of spin and charge in the two regimes.

At the given accuracy of our finite-size extrapolation $M^{-1/2} \to 0$, stating error bars on T^* is challenging. We find our numerics to be most consistent with $T^* = 0.65(5) J_z$.

Effective parton model. To obtain physical insight into our numerical results, we compare them with predictions by an effective parton model [29,30] of the t-J_z model [22]. First we note that the initial creation of the hole changes both the spin and charge quantum numbers, associated with the two global U(1) symmetries of the t-J_z model, by 1; the initial state thus corresponds to a local spinon-chargon pair.

In the subsequent dynamics, the chargon can move by distorting the surrounding spins. Since the Ising interaction is classical and generates no dynamics of its own, the spinon remains localized at the origin. Hence the resulting spin configuration is determined entirely by the chargon's path; different paths may be assumed to be distinguishable up to self-retracing components, since they will lead to different spin configurations in the majority of the cases. That is, the chargon motion effectively creates a memory of the hole's path through the spin background, in the form of a (sometimes called geometric) string Σ of displaced spins connecting the spinon to the chargon. At low temperatures, most strings lead to an increase in the net classical Ising energy $\hat{\mathcal{H}}_{J_z}$, which acts as a potential energy, or string tension, for the chargon.

Formally, in our effective parton model we replace the original t-J_z Hilbert space by a space spanned by orthogonal string states $|\Sigma\rangle$ with the spinon in the origin. States $|\Sigma\rangle$ in the effective Hilbert space correspond to unique states $|\psi_\Sigma\rangle$ in the t-J_z Hilbert space, but the opposite is not true. The effective Hamiltonian $\hat{\mathcal{H}}_{\rm eff}$ consists of a tunneling term with amplitude t between adjacent strings and a potential energy term including the Ising interactions; see Ref. [31] for a detailed definition. At $T = 0$, the dynamics obtained within this parton model is closely related to Brinkman and Rice's retraceable path approximation [32]; at $T > 0$ we average over thermal initial states $|\Psi^n\rangle$ as before.

Our intuitive physical picture above has its limitations. First, effects of loops are ignored; for example, Trugman loops [24] and their generalizations to Ising configurations other than the Néel state effectively introduce spinon motion. Such processes are very slow and can be treated in a tight-binding approximation [22]. Second, not all physical states $|\psi_\Sigma\rangle$ are orthogonal for different Σ; in particular, if a plaquette along the path of the chargon has ferromagnetically aligned spins, paths along opposite directions around this plaquette are indistinguishable [14,20,21], and the corresponding quantum states have nonzero overlap. Our full numerical simulations introduced earlier systematically include these imperfections by constructing an orthonormalized restricted basis set. The number of iterations M corresponds to the maximum string length $\ell_{\rm max}$ considered in the parton theory.

In Fig. 2 we compare our earlier results with predictions by the effective parton model (dashed curves). We find qualitatively similar behavior; in particular, the transition temperature T^* is correctly captured by the effective model. This allows us to analyze the two qualitatively distinct dynamical regimes below and above T^* within the simpler parton theory next.

Thermal spin-charge deconfinement. Well below the Néel temperature, $T \ll T_N$, some spins will be thermally excited, but magnetic order remains. Here, the hole's movement is restrained in a similar way as for $T = 0$ [23], resulting in confinement of the spinon and the chargon. Around T_N, the short-range correlations between the spins decrease rapidly, which may lead to a profound change in the behavior of the hole since these correlations provide a measure of the energy increase resulting from the chargon's movement. Specifically, the average energy $\langle \hat{\mathcal{H}}_{J_z} \rangle_\ell$ of a string with length ℓ, i.e., the string tension, is determined by local spin correlations [22]. Notably, this does not imply that any change of behavior happens at exactly T_N, which is only a measure of long-distance correlations that do not directly affect the chargon's motion. Instead, the dynamical behavior changes at $T^* \neq T_{\rm N}$ in general (although T^* and $T_{\rm N}$ are closely related).

We can estimate T^* by considering the interplay of energy E and entropy S of string states in the effective parton model and ignoring quantum fluctuations $\propto t$. Taylor-expanding the string energy after averaging over the thermal spin background and different string configurations with the same length ℓ allows us to write $E(\ell) \simeq \langle \hat{\mathcal{H}}_{J_z} \rangle_\ell = E_0 + \ell\sigma + \ell^2\sigma'/2 + \cdots$. Assuming a microcanonical ensemble of strings, where all states of a given length ℓ are occupied equally, the entropy becomes $S \simeq \ell \ln(z-1)$, where z is the coordination number of the lattice ($z = 4$ in the 2D square lattice we consider). Hence the free energy

$$F = E - TS \simeq E_0 + \ell(\sigma - T \ln(z-1)) \tag{3}$$

is minimized for $\ell = 0$ (confined partons) when $T < T^*$ and for $\ell \to \infty$ (deconfined partons) when $T > T^*$. The thermal deconfinement transition takes place at

$$T^* = \sigma / \ln(z-1). \tag{4}$$

This picture is expected to remain true when quantum fluctuations $\propto t$ are included. In this case, the individual eigenstates of the Hamiltonian will be Stark localized by the linear string potential for any t/J_z. Although this adds string-length fluctuations, the energy spectrum should remain qualitatively unchanged, with a similar exponential increase in the number of states whose energy is dominated by the potential term $E(\ell)$. Hence we predict T^* independent of t/J_z, as confirmed by our numerical studies above.

As emphasized above, the string tension σ depends only on the local spin correlations. Since these depend on temperature, Eq. (4) needs to be solved self-consistently for T^* with $\sigma = \sigma(T^*)$. Using this procedure, we predict $T^* = 0.65J_z$, remarkably close to the observed value.

Another consequence of Eq. (4) is that T^* becomes small in higher dimensions. In a d-dimensional hypercubic lattice, $z = 2d$; since $\sigma = O(T_N)$ is on the order of the Néel temperature, $T^*/T_N \simeq 1/\ln(d) \to 0$. Hence we expect that T^* is systematically below T_N in high dimensions, further supporting our claim that the observed change in dynamical behavior at T^* is not a mere reflection of the Ising transition at T_N.

Thermalization dynamics. Finally, we study how the mobile hole reaches a steady state when it spreads and interacts with the spin background. One would generically expect the isolated charge to equilibrate to a thermal state at the same temperature T as the Ising spins. However, we observe pronounced deviations from this expected behavior. In a finite-size system, the final temperature should be slightly increased above T to account for the extra kinetic energy added in the quench, but since we use a truncated basis it is difficult to describe this effect quantitatively.

In Fig. 3 we calculate the average kinetic energy $\langle \hat{\mathcal{H}}_t \rangle$ of the hole, defining a local observable, which quickly relaxes to a steady state in a few tunneling times. Next we compare the steady-state result with a thermal ensemble at temperature T. To this end, we sample $n = 1 \cdots N$ thermal background spin configurations $|\Psi^n\rangle$ as described above, introduce a hole, and apply a finite-temperature Lanczos method [33] to describe the hole separately for each n. The thermal average of $N^{-1} \sum_n \langle \hat{\mathcal{H}}_t \rangle_n$ over all samples n is shown in Fig. 3.

At high temperatures, $T \gtrsim T^*$, the thermal ensemble deviates significantly from the steady state for both considered values of t/J_z. Within the effective parton model we attribute this behavior to the fact that the free energy is strongly dominated by the entropic contributions from a large number of long-string states when $T > T^*$. Hence, in the postquench dynamics the chargon can quickly populate these long-string states, which leads to the observed steady-state behavior. We expect that much longer times would be required for the local kinetic energy to equilibrate too. We checked this picture by calculating string-length distributions and find that they quickly resemble the thermal ensemble [31].

At low temperatures, $T \lesssim T^*$, we see in Fig. 3 that $\langle \hat{\mathcal{H}}_t \rangle$ becomes thermal for $t/J_z = 1$, whereas it remains nonthermal for larger $t/J_z = 3$ at the considered times. In the latter case we believe that the significant separation of time scales in combination with the discrete spectrum of the Ising background leads to excessive thermalization times. To exchange energy with the spin environment, the chargon has to perform loops, which requires overcoming high energy barriers [24].

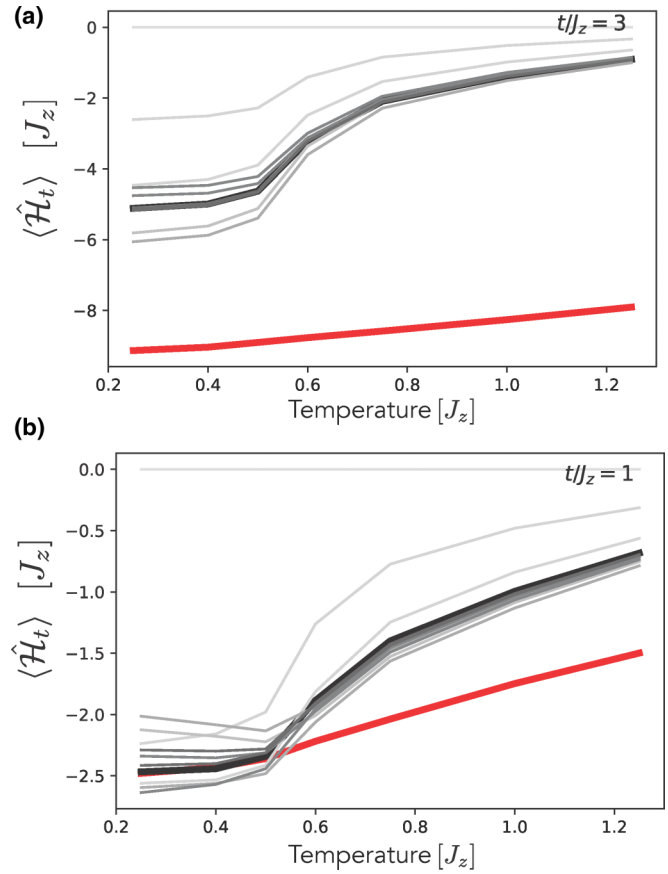

FIG. 3. The mobile dopant reaches a steady state (black) over a few tunneling times, as can be seen from its average kinetic energy $\langle \hat{\mathcal{H}}_t \rangle$. We consider (a) $t/J_z = 3$ and (b) $t/J_z = 1$ and use the truncated-basis method described in the text. The gray curves are the expectation value at earlier times, starting at $\tau = 0$ and increasing in steps of $\Delta\tau = 1/t$. The steady-state value (black) was obtained by averaging over times $\tau = 10/t$ to $15/t$. Comparison of our results with a thermal ensemble (red) at the same temperature T as the spin background shows that the steady state is pronouncedly nonthermal in many cases.

Indeed at low temperatures we find signatures for unoccupied loop states in the hole dynamics, which would be occupied in the thermal ensemble [31].

Summary and outlook. We have established two temperature regimes $T \lessgtr T^*$ with distinct dynamical behavior of an initially localized hole moving in an Ising antiferromagnet. The observed dynamical transition at T^* can be interpreted as thermal spinon-chargon deconfinement. Although we find a true phase transition in an effective parton model, we cannot distinguish with certainty between a crossover and a true transition around T^* in our fully numerical data of the microscopic t-J_z model. While we cannot distinguish the deconfinement temperature $T^*|_{2D} \gtrsim T_N$ from the Néel temperature T_N in our 2D simulations with absolute certainty, we expect from analytical arguments that $T^* < T_N$ in higher dimensions. Furthermore, we studied thermalization dynamics of a single hole in the t-J_z model and revealed stable steady states with nonthermal properties in both the confined and deconfined regimes.

Our theoretical analysis can be tested and extended experimentally using ultracold atoms in optical lattices [12]. To realize the required Ising interactions, Rydberg dressing appears to be the most promising candidate. In particular, this allows one to realize AFM couplings for bosons [34,35] or fermions [36]. For a single dopant the quantum statistics plays no role, extending the number of existing experimental setups that can address the quench dynamics studied in this Research Letter. Hence another possibility is to use spin-dependent interactions [37–39] to realize a bosonic model with AFM couplings.

In the future, similar studies of the SU(2) invariant t-J model at finite temperature will be interesting. Experimentally, it is also conceivable to address hole dynamics at nonzero hole densities. Another interesting direction would be to explore thermalization dynamics of a single hole in the t-J_z model at much longer times than addressed here. This may be possible using a combination of classical Monte Carlo sampling of the Ising background, as performed here, with large-scale time-dependent numerical density matrix renormalization group (or tensor-network) simulations on extended cylinders [15,18].

Acknowledgments. We thank E. Demler, U. Schollwöck, F. Palm, M. Knap, M. Greiner, M. Lebrat, G. Ji, M. Kanasz-Nagy, I. Lovas, Y. Wang, S. Ding, L. Rammelmüller, L. Pollet, I. Bloch, and I. Cirac for fruitful discussions. The authors acknowledge funding from the European Research Council (ERC) under the European Union's Horizon 2020 research and innovation program (Grant Agreement No. 948141), by the Deutsche Forschungsgemeinschaft (DFG, German Research Foundation) under Germany's Excellence Strategy–EXC-2111–390814868, by the NSF through a grant for the Institute for Theoretical Atomic, Molecular, and Optical Physics at Harvard University, and by the Smithsonian Astrophysical Observatory.

[1] P. A. Lee, N. Nagaosa, and X. G. Wen, Doping a Mott insulator: Physics of high-temperature superconductivity, Rev. Mod. Phys. **78**, 17 (2006).
[2] J. Koepsell, D. Bourgund, P. Sompet, S. Hirthe, A. Bohrdt, Y. Wang, F. Grusdt, E. Demler, G. Salomon, C. Gross, and I. Bloch, Microscopic evolution of doped Mott insulators from polaronic metal to Fermi liquid, Science **374**, 82 (2021).
[3] B. I. Shraiman and E. D. Siggia, Two-Particle Excitations in Antiferromagnetic Insulators, Phys. Rev. Lett. **60**, 740 (1988).
[4] C. L. Kane, P. A. Lee, and N. Read, Motion of a single hole in a quantum antiferromagnet, Phys. Rev. B **39**, 6880 (1989).
[5] S. Sachdev, Hole motion in a quantum Néel state, Phys. Rev. B **39**, 12232 (1989).
[6] E. Dagotto, R. Joynt, A. Moreo, S. Bacci, and E. Gagliano, Strongly correlated electronic systems with one hole: Dynamical properties, Phys. Rev. B **41**, 9049 (1990).
[7] G. Martinez and P. Horsch, Spin polarons in the t-J model, Phys. Rev. B **44**, 317 (1991).
[8] Z. Liu and E. Manousakis, Dynamical properties of a hole in a Heisenberg antiferromagnet, Phys. Rev. B **45**, 2425 (1992).
[9] M. Brunner, F. F. Assaad, and A. Muramatsu, Single-hole dynamics in the $t-J$ model on a square lattice, Phys. Rev. B **62**, 15480 (2000).
[10] F. Grusdt, A. Bohrdt, and E. Demler, Microscopic spinon-chargon theory of magnetic polarons in the t-J model, Phys. Rev. B **99**, 224422 (2019).
[11] K. K. Nielsen, M. A. Bastarrachea-Magnani, T. Pohl, and G. M. Bruun, Spatial structure of magnetic polarons in strongly interacting antiferromagnets, Phys. Rev. B **104**, 155136 (2021).
[12] A. Bohrdt, L. Homeier, C. Reinmoser, E. Demler, and F. Grusdt, Exploration of doped quantum magnets with ultracold atoms, Ann. Phys. (Amsterdam) **435**, 168651 (2021).
[13] J. Koepsell, J. Vijayan, P. Sompet, F. Grusdt, T. A. Hilker, E. Demler, G. Salomon, I. Bloch, and C. Gross, Imaging magnetic polarons in the doped Fermi-Hubbard model, Nature (London) **572**, 358 (2019).
[14] G. Ji, M. Xu, L. H. Kendrick, C. S. Chiu, J. C. Brüggenjürgen, D. Greif, A. Bohrdt, F. Grusdt, E. Demler, M. Lebrat, and M. Greiner, Coupling a Mobile Hole to an Antiferromagnetic Spin Background: Transient Dynamics of a Magnetic Polaron, Phys. Rev. X **11**, 021022 (2021).
[15] A. Bohrdt, F. Grusdt, and M. Knap, Dynamical formation of a magnetic polaron in a two-dimensional quantum antiferromagnet, New J. Phys. **22**, 123023 (2020).
[16] M. Mierzejewski, L. Vidmar, J. Bonča, and P. Prelovšek, Nonequilibrium Quantum Dynamics of a Charge Carrier Doped into a Mott Insulator, Phys. Rev. Lett. **106**, 196401 (2011).
[17] D. Golež, J. Bonča, M. Mierzejewski, and L. Vidmar, Mechanism of ultrafast relaxation of a photo-carrier in antiferromagnetic spin background, Phys. Rev. B **89**, 165118 (2014).
[18] C. Hubig, A. Bohrdt, M. Knap, F. Grusdt, and J. I. Cirac, Evaluation of time-dependent correlators after a local quench in iPEPS: hole motion in the t-J model, SciPost Phys. **8**, 021 (2020).
[19] A. Bohrdt, E. Demler, F. Pollmann, M. Knap, and F. Grusdt, Parton theory of angle-resolved photoemission spectroscopy spectra in antiferromagnetic Mott insulators, Phys. Rev. B **102**, 035139 (2020).
[20] J. Carlström, N. Prokof'ev, and B. Svistunov, Quantum Walk in Degenerate Spin Environments, Phys. Rev. Lett. **116**, 247202 (2016).
[21] M. Kanász-Nagy, I. Lovas, F. Grusdt, D. Greif, M. Greiner, and E. A. Demler, Quantum correlations at infinite temperature: The dynamical Nagaoka effect, Phys. Rev. B **96**, 014303 (2017).
[22] F. Grusdt, M. Kánasz-Nagy, A. Bohrdt, C. S. Chiu, G. Ji, M. Greiner, D. Greif, and E. Demler, Parton Theory of Magnetic Polarons: Mesonic Resonances and Signatures in Dynamics, Phys. Rev. X **8**, 011046 (2018).
[23] L. N. Bulaevskii, É. L. Nagaev, and D. I. Khomskii, A new type of auto-localized state of a conduction electron in an antiferromagnetic semiconductor, J. Exp. Theor. Phys. **27**, 836 (1968).
[24] S. A. Trugman, Interaction of holes in a Hubbard antiferromagnet and high-temperature superconductivity, Phys. Rev. B **37**, 1597 (1988).
[25] A. L. Chernyshev and P. W. Leung, Holes in the $t-J_z$ model: A diagrammatic study, Phys. Rev. B **60**, 1592 (1999).

[26] C. S. Chiu, G. Ji, A. Bohrdt, M. Xu, M. Knap, E. Demler, F. Grusdt, M. Greiner, and D. Greif, String patterns in the doped Hubbard model, Science **365**, 251 (2019).

[27] D. Poilblanc, H. J. Schulz, and T. Ziman, Single hole in a quantum antiferromagnet: Finite-size-scaling approach, Phys. Rev. B **46**, 6435 (1992).

[28] L. Vidmar and J. Bonča, Real-time current of a charge carrier in a strongly correlated system coupled to phonons, driven by a uniform electric field, J. Supercond. Novel Magn. **25**, 1255 (2012).

[29] P. Coleman, New approach to the mixed-valence problem, Phys. Rev. B **29**, 3035 (1984).

[30] P. Béran, D. Poilblanc, and R. B. Laughlin, Evidence for composite nature of quasiparticles in the 2D t-J model, Nucl. Phys. B **473**, 707 (1996).

[31] See Supplemental Material at http://link.aps.org/supplemental/10.1103/PhysRevB.105.L241113 for details.

[32] W. F. Brinkman and T. M. Rice, Single-Particle Excitations in Magnetic Insulators, Phys. Rev. B **2**, 1324 (1970).

[33] J. Jaklič and P. Prelovšek, Lanczos method for the calculation of finite-temperature quantities in correlated systems, Phys. Rev. B **49**, 5065 (1994).

[34] J. Zeiher, R. van Bijnen, P. Schausz, S. Hild, J.-y. Choi, T. Pohl, I. Bloch, and C. Gross, Many-body interferometry of a Rydberg-dressed spin lattice, Nat. Phys. **12**, 1095 (2016).

[35] J. Zeiher, J.-y. Choi, A. Rubio-Abadal, T. Pohl, R. van Bijnen, I. Bloch, and C. Gross, Coherent Many-Body Spin Dynamics in a Long-Range Interacting Ising Chain, Phys. Rev. X **7**, 041063 (2017).

[36] E. Guardado-Sanchez, B. M. Spar, P. Schauss, R. Belyansky, J. T. Young, P. Bienias, A. V. Gorshkov, T. Iadecola, and W. S. Bakr, Quench Dynamics of a Fermi Gas with Strong Nonlocal Interactions, Phys. Rev. X **11**, 021036 (2021).

[37] L. M. Duan, E. Demler, and M. D. Lukin, Controlling Spin Exchange Interactions of Ultracold Atoms in Optical Lattices, Phys. Rev. Lett. **91**, 090402 (2003).

[38] S. Trotzky, P. Cheinet, S. Fölling, M. Feld, U. Schnorrberger, A. M. Rey, A. Polkovnikov, E. A. Demler, M. D. Lukin, and I. Bloch, Time-resolved observation and control of superexchange interactions with ultracold atoms in optical lattices, Science **319**, 295 (2008).

[39] I. Dimitrova, N. Jepsen, A. Buyskikh, A. Venegas-Gomez, J. Amato-Grill, A. Daley, and W. Ketterle, Enhanced Superexchange in a Tilted Mott Insulator, Phys. Rev. Lett. **124**, 043204 (2020).